TÜBİTAK

Turkish Journal of Chemistry

http://journals.tubitak.gov.tr/chem/

Research Article

Turk J Chem
(2018) 42: 505 – 519

doi:10.3906/kim-1706-63

Removal of five cationic dyes using a resin coated with nickel/nickel boride nanoparticles

Merve ÇINAR, Yasemin İŞLEK COŞKUN*, Tülin DENİZ ÇİFTÇİ
Department of Chemistry, Faculty of Science, Ege University, Bornova, İzmir, Turkey

Received: 29.06.2017 • **Accepted/Published Online:** 25.12.2017 • **Final Version:** 27.04.2018

Abstract: Resins coated with nickel/nickel boride nanoparticles were used to remove brilliant green, methyl violet, methylene blue, phenosafranine, and brilliant cresyl blue from water. The effects of pH, adsorbent dose, contact time, and initial dye concentration on the adsorption efficiencies were investigated. The point of zero charge for the adsorbent was pH 9.5. Isotherm studies were conducted using Langmuir, Freundlich, and Dubinin–Radushkevich models, and thermodynamic studies were also performed. Adsorption of the five dyes was found to obey the Langmuir isotherm model and was endothermic. The maximum adsorption capacities calculated from the Langmuir isotherm were 66.7, 88.5, 144.9, 56.2, and 147.1 mg/g for methylene blue, brilliant cresyl blue, methyl violet, phenosafranine, and brilliant green, respectively. E values obtained from the Dubinin–Radushkevich isotherm showed that the adsorption mechanism was chemical in nature. Furthermore, three kinetic models (pseudo first-order, pseudo second-order, and intraparticle) were investigated. The pseudo second-order kinetic model fit the five cationic dyes best.

Key words: Nanoparticles, removal, dye, spectrophotometry

1. Introduction

Humans have been using dyes since antiquity.[1] Almost everything is colored using dyes, including food, furniture, textiles, and cosmetics.[2,3] Although dyes aesthetically contribute to materials, they also cause severe environmental problems when they are released into industrial wastewaters.[3] The effluents are toxic and affect both aquatic life and human health. Furthermore, dyes prevent sunlight from penetrating into the water and increase the chemical oxygen demand of the effluents.[4–7] Hence, the removal of the dyes before discharge is a crucial step for environmental safety.

Dyes can be categorized into three groups: anionic, cationic, and nonionic. Brilliant green (BG), methyl violet (MV), methylene blue (MB), phenosafranine (PS), and brilliant cresyl blue (BCB) are all cationic dyes. Cationic dyes are known to be more toxic than anionic dyes.[2] Such dyes are frequently used in the manufacturing of inks, paints, indicators, reagents, cosmetics, food, paper, and textiles.[8–11] Additionally, MV and PS are used as biological stains[9,11] PS is also used in redox probes and as a photosensitizer.[12] These five cationic dyes can cause skin damage and severe eye damage and are toxic to aquatic life. Direct human exposure may also cause diarrhea, abdominal pain, difficulty in breathing, nausea, vomiting, and jaundice.[8,9,11,13]

Various techniques have been used for dye removal including sedimentation, filtration, oxidation, elec-

*Correspondence: yasemin.islek@ege.edu.tr

trochemical processes, adsorption, and ion exchange.[1,14] Among them, adsorption provides specific advantages such as high removal capacity, low cost, practical implementation, and design simplicity.[15,16] The most commonly used adsorbents for dye removal include natural clay minerals, siliceous materials, zeolites, agricultural wastes, industrial by-products, activated carbon, bio-based materials, and polymeric materials.[15] Recently, reports on dye removal using nanomaterials have increased. Furthermore, combining nanomaterials with magnetic separation techniques has provided specific advantages, such as fast and effective separation. Tea waste loaded with magnetite nanoparticles was used for the removal of seven dyes (Janus green, Congo red, thionine, neutral red, MB, reactive blue 19, and crystal violet) by Madrakian et al.[17] The adsorption reached maximum with 0.02 g of the adsorbent for cationic dyes and the maximum percentage removal was about 98%. The optimum contact time was found to be 35 min. The capacities of Janus green, Congo red, thionine, neutral red, MB, reactive blue 19, and crystal violet were reported as 129.87, 82.64, 128.21, 126.58, 119.05, 87.72, and 113.64 mg/g, respectively. Adsorption data fit the Langmuir model for all dyes. MB, BCB, and neutral red were removed using magnetic multiwall carbon nanotube nanocomposites by Gong et al.[18] The optimum sorbent dose was 0.5 g/L and the contact time was 24 h. The data for MB, BCB, and neutral red fit the Freundlich model. The results showed that the capacity values for the adsorption of MB, neutral red, and BCB by the magnetic nanocomposites were 15.74, 20.33, and 23.55 mg/g, respectively. Magnetic alginate beads containing activated carbon were developed to remove MB and methyl orange by Rocher et al.[19] In order to reach equilibrium, 180 min was required. The Langmuir isotherm model was applied. The maximum capacities were 38.9 mmol/g for the activated carbon part and 0.059 mmol/g for beads for MB and 1.32 mmol/g for the activated carbon part and 0.003 mmol/g for beads for methyl orange. Hosseini et al. synthesized three magnetic chitosan nanocomposites (Fe_3O_4–chitosan, Fe_3O_4–chitosan–tripolyphosphate, Fe_3O_4–chitosan–glutaraldehyde) and evaluated their efficiencies on methyl orange removal.[20] It was found that the Fe_3O_4–chitosan–glutaraldehyde nanogel adsorbent showed a faster adsorption rate toward methyl orange compared to the other nanoadsorbents. The maximum adsorption capacity was 20.5 mg/g. The adsorption obeyed the Langmuir isotherm model.

Magnetic adsorbents based on functionalized graphene oxide were developed and utilized for removing crystal violet and MB by Sahraei et al.[21] The adsorption results obeyed the Langmuir isotherm. The maximum adsorption capacities were 416.06 and 440.97 mg/g for MB and crystal violet, respectively. Mahmoodi et al. investigated the removal of direct red 23, direct red 31, and direct green 6 dyes using zinc ferrite nanoparticles.[22] It was found that dye adsorption fit the Langmuir isotherm. The optimum adsorbent amount was 400 mg. The maximum adsorption capacities were 26.1, 55.5, and 64.1 mg/g for direct red 23, direct red 31, and direct green 6, respectively. The dye removal efficiency was reported to reach maximum values (51%, 27%, and 23% for direct red 31, direct green 6, and direct red 23, respectively) after 60 min of contact time.

When the studies on dye removal in the literature are examined, it is understood that the preparation step of many adsorbents is quite long and complicated. However, a large amount of toxic chemical is used to prepare sorbent. Furthermore, the time required for highly efficient dye removal is quite long. Even when a high amount of adsorbent is used to achieve maximum removal efficiency, efficiency cannot be greatly increased. In many studies, the adsorption capacity is also not high.

Recently, Çiftçi and Henden used nickel/nickel boride nanoparticle-coated resin (Ni/Ni_xB-NPCR) for the removal of arsenic from water.[23] The present study is the first to use Ni/Ni_xB-NPCR for dye removal. This study aimed to develop a fast, reliable, and simple technique for the removal of cationic dyes based on spectrophotometric measurements. The effects of experimental parameters such as pH, adsorbent dose, contact

time, and initial dye concentration were examined. Isothermic, thermodynamic, and kinetic parameters were also evaluated. The method was applied successfully to the removal of cationic dyes from model solutions.

2. Results and discussion

2.1. Characterization of the adsorbent

Çiftçi and Henden previously characterized Ni/Ni_xB-NPCR using scanning electron microscopy combined with X-ray energy dispersive spectrometry (EDX), atomic force microscopy (AFM), and X-ray electron spectrometry.[23] Furthermore, the Ni/Ni_xB layer was analyzed in detail in another previous study.[24] According to the AFM analysis, the diameters of the Ni/Ni_xB nanoparticles on the resin were in the range of 18 nm to 50 nm. EDX analysis showed that the particles consisted of nickel, boron, oxygen, and carbon. The amounts of nickel and boron in the coating layer were also determined using a flame atomic absorption spectrometer and the spectrophotometric azomethine method, respectively. The amounts of nickel and boron were found to be 49.20 ± 0.02 and 3.17 ± 0.32 mg/g, respectively.

2.2. The effect of pH

The effect of pH on the removal efficiencies was studied in the pH range of 3–10 for all dyes. The removal efficiencies of MB, PS, BG, MV, and BCB are presented in Figure 1a. The final pH of the dye solution increased to almost 9 after adsorption, regardless of the initial pH. As shown in Figure 1a, the removal efficiencies were not significantly affected by the initial pH, and the removal efficiencies were 75%–87%, 88%–97%, 92%–97%, 97%–98%, and 87%–95% for MB, PS, BG, MV, and BCB, respectively.

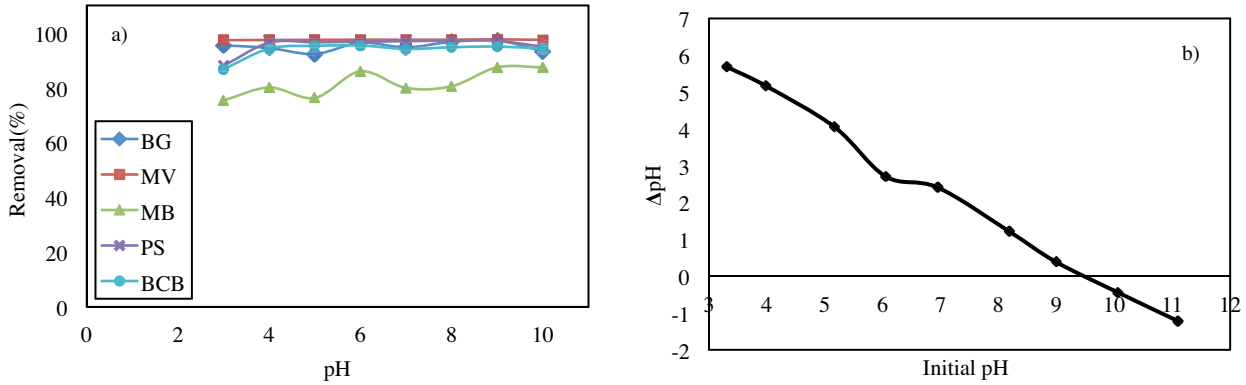

Figure 1. a) The initial pH effect for the removal of MB, PS, BG, MV, and BCB (pH range: 3–10, sorbent amount: 10 mg, initial dye concentration: 20 mg/L, volume: 25 mL, shaken for 24 h at 25 °C); b) zero point charge of pH of the sorbent (pH range: 3–11; sorbent amount: 10 mg; solution 25 mL of 0.1 mol/L KNO_3; shaken for 24 h at 25 °C; ΔpH = final pH – initial pH).

2.3. Determination of the point of zero charge

Study of the pH of the point of zero charge (pH_{pzc}) of the adsorbent gave information about the adsorption process. The pH_{pzc} is defined as the pH value at which the charge of the positive surface sites is equal to the negative surface sites. Determining the pH_{pzc} identifies possible electrostatic interactions between adsorbent and dye molecules. The surface of the adsorbent was negatively charged and could interact with the positively

charged species when the solution pH was higher than the pH_{pzc}. Conversely, at pH values lower than the pH_{pzc}, the surface of the adsorbent is positively charged and should only interact with negatively charged species.[25] The pH_{pzc} of the adsorbent is shown in Figure 1b and was found to be 9.5. It was expected that the removal efficiencies would be low in acidic solutions because of the electrostatic repulsion between the positively charged adsorbent and the positively charged dye molecules. However, the removal efficiencies were high at pH values both lower and higher than the pH_{pzc}. Considering that all of the final solution pH values were above 9 and independent of the initial pH, the surface of the adsorbent was negatively charged. Therefore, the adsorption mechanism was based on electrostatic attraction. Similar electrostatic interactions for dye removal have been reported for BG removal using an amine-modified tannin gel and *Peganum harmala* activated carbon, MV removal using magnetic walnut shells and nanostructured carbon-covered sand, and MB removal using magnetic particles loaded with activated carbon.[26– 30]

2.4. The effect of adsorbent dose

The effect of adsorbent dose on the removal efficiency was investigated and is shown in Figure 2. The graph shows that the removal efficiencies increased by increasing the adsorbent dose and reached a constant value. The removal efficiencies reached 99.3% for BG at 1.2 g/L, 97.6% for PS at 1.8 g/L, 98.8% for MB at 1.8 g/L, 91.2% for MV at 2.4 g/L, and 93.8% for BCB at 2.4 g/L. The optimum adsorbent doses were selected for further studies as 1.2 g/L for BG, 1.8 g/L for PS and MB, and 2.4 g/L for BCB and MV. The removal efficiency increase for dyes could be explained by increasing the number of adsorption sites on the adsorbent. In other words, the high removal efficiency at higher adsorbent doses was due to the increased number of available adsorption sites.[31,32] Similar patterns have been observed for MV removal using magnetic walnut shells, MB removal using magnetic particles loaded with activated carbon, and BG removal using *Peganum harmala* activated carbon.[27,28,30]

2.5. The effect of contact time

The correlations between contact time and dye removal efficiency were examined. As shown in Figure 3, the removal rate was high during the first minute. The removal efficiencies reached a plateau after 60 min for PS, MB, and BG and after 240 min for BCB and MV. The high adsorption rate at the beginning may be by virtue of the presence of uncovered sites on the adsorbent surface. Furthermore, the fast removal of the dyes from water could be the result of electrostatic interactions between the negatively charged adsorbent surface and the positively charged dye molecules.[33] However, as the adsorption process continues, all existing adsorption areas are gradually engaged by the dye molecules.[31,32] Similar observations were reported by Akter et al. and Agarwal et al. for BG removal, Ashrafi et al. and Moradi and Azizian for MV removal, and Altıntıg et al. for MB removal.[26–30]

2.6. The effect of initial dye concentration

Dye solutions at different concentrations (5, 10, 25, 50, 100, 200, and 400 mg/L) were added to the adsorbents and shaken. The removal efficiencies versus the initial concentrations are shown in Figure 4. The removal efficiencies increased as the initial dye concentration increased until a plateau was reached. Thereafter, the removal efficiencies started to decrease with increasing initial dye concentration. Adsorbents have a certain number of active sites and they become completely occupied after certain dye concentrations are exceeded.[34] When the adsorbent cannot provide sufficient unoccupied sites to adsorb all of the dye molecules in the solution, such a decrease emerges[35] This phenomenon occurs as a result of adsorbent surface saturation.[7] The optimum

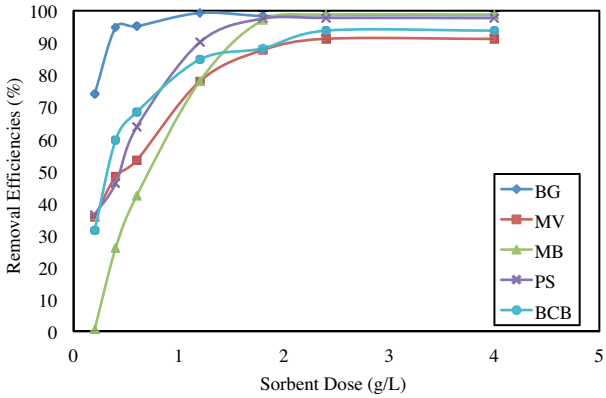

Figure 2. The adsorbent dose effect for the removal of MB, PS, BG, MV, and BCB (initial concentration: 20 mg/L; volume: 25 mL; contact time: 24 h at 25 °C; pH: 4).

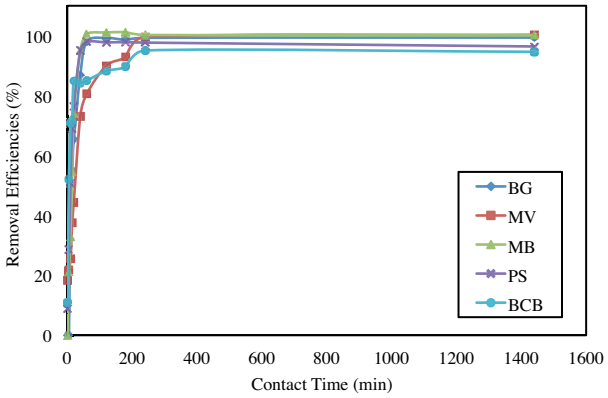

Figure 3. The contact time effect for the removal of MB, PS, BG, MV, and BCB (initial concentration: 20 mg/L; volume: 25 mL; adsorbent dose: 1.2 g/L for BG, 1.8 g/L for PS and MB, 2.4 g/L for BCB and MV; temperature: 25 °C; pH: 4).

initial dye concentrations were determined to be 100 mg/L for BG (98.3%), MV (98.4%), and PS (98.9%) and 50 mg/L for MB (99.6%) and BCB (96.8%).

2.7. The effect of temperature on the removal efficiencies

With the optimum parameters in hand, temperature effects on the removal efficiencies of the five cationic dyes were studied at 298 K, 303 K, 313 K, and 323 K. Figure 5 shows the graph of removal efficiencies versus temperature. The removal efficiencies increased as the temperature increased until a plateau was reached. These increases showed that the adsorption was endothermic. The endothermic nature of the adsorption was also verified by the adsorption thermodynamic studies in Section 2.8. The increased temperature can enhance the rate of dye molecules and decrease in the viscosity of the solution and the diffusion rates of the dye molecules increase through the external boundary layer.[14] Fil et al., Özdemir et al., Kismir and Aroguz, and Mandal and Ray reported that the adsorption of MV, MB, BG, and BCB was endothermic.[36–39]

2.8. Adsorption kinetic studies

Kinetic studies are important for research into adsorption parameters because they help determine the potential applications of the adsorbent.[40] Adsorption kinetics can be evaluated using reaction- and diffusion-based models. The linearized pseudo first-order and pseudo second-order kinetic equations are described by Eqs. (1) and (2), respectively:

$$log\,(q_e - q_t) = log\,q_e - \frac{k_1 t}{2.303} \tag{1}$$

$$\frac{t}{q_t} = \frac{1}{k_2\,q_e^2} + \frac{t}{q_e} \tag{2}$$

Here, q_e and q_t indicate the adsorption capacity at equilibrium (mg/g) and at time t, respectively; k_1 and k_2 are the pseudo first-order (1/min) and pseudo second-order rate constants (g/mg min), respectively.

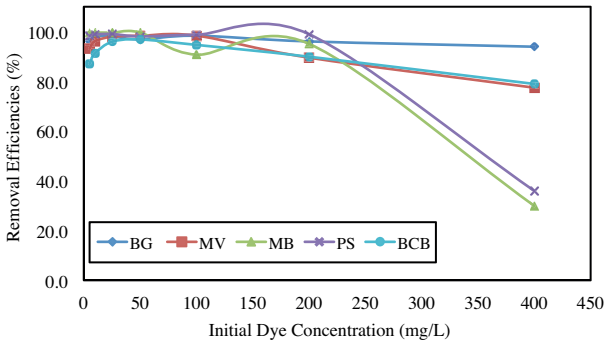

Figure 4. The initial dye concentration effect for the removal of MB, PS, BG, MV, and BCB (volume: 25 mL; contact time: 60 min for PS, MB, and BG and 240 min for BCB and MV at 25 °C; adsorbent dose: 1.2 g/L for BG, 1.8 g/L for PS and MB, 2.4 g/L for BCB and MV; pH: 4).

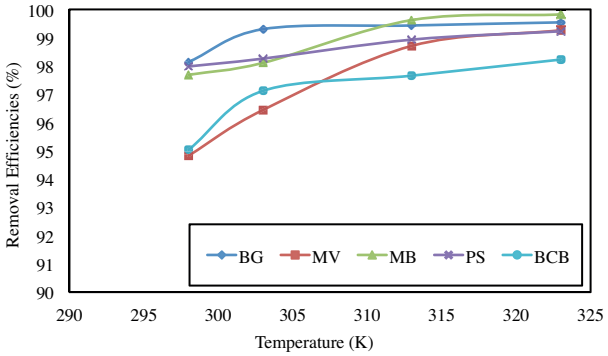

Figure 5. The temperature effect for the removal of MB, PS, BG, MV, and BCB (initial concentrations: 100 mg/L for BG, MV, and PS and 50 mg/L for MB and BCB; volume: 25 mL; contact time: 60 min for PS, MB, and BG and 240 min for BCB and MV at 25 °C; adsorbent dose 1.2 g/L for BG, 1.8 g/L for PS and MB, 2.4 g/L for BCB and MV; pH: 4).

Given that these kinetic models are inefficient at providing information about the reaction mechanism, a diffusion-based model was also studied. The intraparticle diffusion model was evaluated as follows:

$$q_t = k_{int} t^{0.5} + I \tag{3}$$

Here, t is the contact time (min) and k_{int} (mg/g $\min^{0.5}$) and I (mg/g) are the intraparticle diffusion constants. When the plots of q_t versus $t^{0.5}$ are drawn with the experimental data, a linear relationship that passes through the origin is seen; this relationship indicates that the adsorption processes are entirely based on intraparticle diffusion. When the plot does not pass through the origin but still has a linear slope, a mechanism involving the external mass transfer or chemical adsorption is valid[41] When multilinear plots are obtained, multiple association stages are possible. I is the intercept of the linear equation and defines the thickness of the boundary layer. The boundary layer effect increases with increasing intercept value.[38] Under the intensive shaking conditions during the adsorption process, the intraparticle diffusion of dyes from solution to adsorbent surface is generally a limiting step.[18]

Figures 6a–6d show the effect of time on the adsorption efficiency and the linearized pseudo first-order, pseudo second-order, and intraparticle diffusion kinetic models. Kinetic constants belonging to the pseudo first-order, pseudo second-order, and intraparticle diffusion kinetic models are shown in Tables 1 and 2.

The pseudo first-order constants were calculated using the intercept and the slope of the graph of ln $(q_e - q_t)$ versus time. The correlation coefficients of the graphs were found to be low (0.9007 for MB, 0.9725 for BG, 0.5705 for BCB, 0.9849 for PS, and 0.9810 for MV), and the experimental q values of the dye were not close to the calculated q values. Hence, the pseudo first-order model was not applicable. As shown in Table 1 and Figure 6, the maximum correlation coefficients for the dyes were obtained with the pseudo second-order equations. Therefore, the pseudo second-order kinetic model led to the adsorption kinetics of MB, BG, BCB, PS, and MV. This result indicates that the rate-limiting step of the adsorption process was chemisorption.[14] Chemical adsorption, which contains valence forces through the sharing or exchange of electrons between adsorbent and dye molecules, may control the adsorption process.[42] Moreover, the values of $q_{e,calc}$ and $q_{e,exp2}$ were close

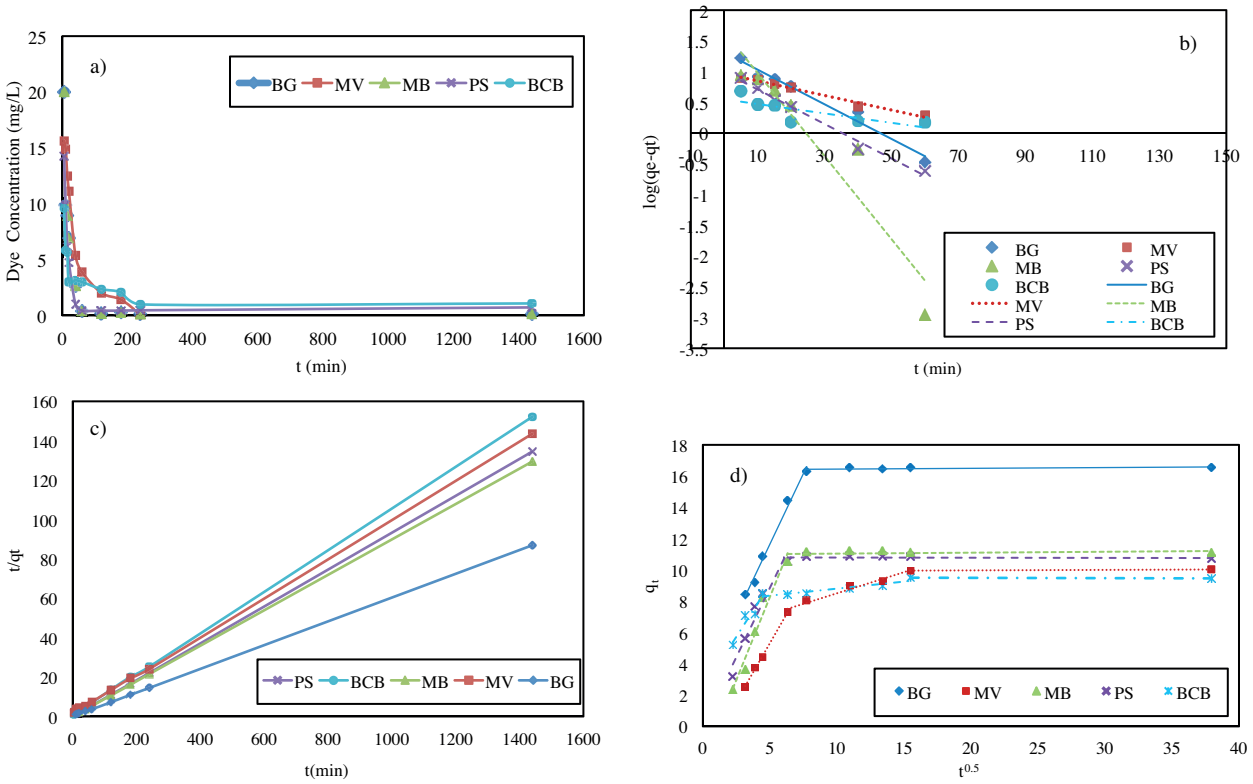

Figure 6. Kinetic studies for MB, PS, BG, MV, and BCB adsorption: a) time effects, b) pseudo first-order kinetic model, c) pseudo second-order kinetic model, d) intraparticle diffusion kinetic model (initial concentrations: 20 mg/L; volume: 25 mL; adsorbent dose: 1.2 g/L for BG, 1.8 g/L for PS and MB, 2.4 g/L for BCB and MV; temperature: 25 °C; pH: 4).

Table 1. The constants of the pseudo first-order and pseudo second-order kinetic models for MB, BG, BCB, PS, and MV adsorption using the magnetic Ni/Ni$_x$B-NPCR.

		Pseudo first-order			Pseudo second-order		
	$q_{e,exp}$ (mg/g)	k_1 (1/min)	$q_{e,calc1}$ (mg/g)	R^2	k_2 (g/mg min)	$q_{e,calc2}$ (mg/g)	R^2
MB	44.46	0.1554	11.11	0.9007	0.01391	11.20	0.9997
BG	20.53	0.06494	16.67	0.9725	0.01051	16.64	0.9999
BCB	2.971	0.009212	10.00	0.5705	0.02309	9.497	0.9999
PS	9.750	0.06471	11.11	0.9849	0.03282	10.75	0.9999
MV	9.270	0.02718	10.00	0.9810	0.005757	10.18	0.9997

to each other and indicated that the pseudo second-order kinetic model fit the experimental data. According to Allen et al.,[43] it is impossible to differentiate between physical adsorption and chemisorption in certain circumstances despite high R^2 values; moreover, in some conditions, both types of adsorption may be active.

In Figure 6d, for the intraparticle model, the graphs did not pass through the origin and indicated that the intraparticle diffusion model did not play an important role. Furthermore, the rate-limiting step may be

Table 2. The constants of intraparticle kinetic model for MB, BG, BCB, PS, and MV adsorption using the magnetic Ni/Ni$_x$B-NPCR.

	Intraparticle model								
	First stage			Second stage			Third stage		
	I_1 (mg/g)	$K_{int,1}$ (mg/g min$^{0.5}$)	R^2	I_2 (mg/g)	$K_{int,2}$ (mg/g min$^{0.5}$)	R^2	I_3 (mg/g)	$K_{int,3}$	R^2
MB	–2.32	2.12	0.955	10.9	0.006	0.073	-	-	-
BG	2.62	1.815	0.990	16.4	0.005	0.349	-	-	-
BCB	2.37	1.35	0.925	7.91	0.090	0.864	9.54	–0.002	1
PS	0.006	1.77	0.937	10.8	–0.001	0.010	-	-	-
MV	–2.13	1.49	0.998	5.81	0.270	0.968	9.91	0.0032	1

a complex combination of chemisorption and intraparticle transport.[41,42] Two linear stages were seen for MB, BG, and PS, whereas three linear stages were observed for BCB and MV. The first stage and the second stage were ascribed to bulk diffusion and intraparticle diffusion, respectively.[38] For BCB and MV, the final stage was the equilibrium stage, which may have been affected by the decrease in intraparticle diffusion because of the low dye concentrations in the solution.[14]

2.9. Thermodynamic studies

Thermodynamic studies provide information about the effect of temperature on the adsorption process. They display the spontaneity, randomness, and endothermicity/exothermicity of the adsorption processes. To calculate the Gibbs free energy changes (ΔG°), enthalpy (ΔH°) and entropy changes (ΔS°), the following equations were used:[38,44]

$$lnK_L = -\frac{\Delta H^o}{RT} + \frac{\Delta S^o}{R} \tag{4}$$

$$\Delta G^o = -RTlnK_L \tag{5}$$

$$K_L = \frac{q_e}{C_e} \tag{6}$$

$$\Delta G^o = \Delta H^o - T\Delta S^o \tag{7}$$

Here, ΔG° is the free energy change (kJ/mol), R is the gas constant (8.314 J/mol K), K_L is the thermodynamic equilibrium constant, and T is temperature (K). K_L values were found from the ratio of the adsorbed dye concentration (mg) and equilibrium dye concentration in solution (mg/L). The parameters of ΔH and ΔS were acquired from the slope and the intercept of the Van't Hoff graph between lnK_L and 1/T, respectively. The value of ΔG° determines whether the adsorption is spontaneous, and a negative value indicates spontaneity.[38] Positive values for ΔH° indicate that the adsorption is endothermic, whereas negative values represent exothermic adsorption. ΔS° values show the degree of disorder or randomness of the adsorption process.[40] The calculated values obtained at 298 K, 303 K, 313 K, and 323 K are listed in Table 3.

Table 3. The constants of thermodynamic model for MB, BG, BCB, PS, and MV adsorption using the magnetic Ni/Ni$_x$B-NPCR.

	T (K)	ΔH° (kJ/mol)	ΔS° (J/mol K)	ΔG° (kJ/mol)
MB	298	67.54	249.8	–6.891
	303			–8.140
	313			–10.64
	323			–13.14
BG	298	17.02	89.37	–9.611
	303			–10.06
	313			–10.95
	323			–11.84
BCB	298	8.028	44.96	–5.368
	303			–5.593
	313			–6.043
	323			–6.492
PS	298	9.983	58.66	–7.497
	303			–7.790
	313			–8.377
	323			–8.963
MV	298	44.03	164.1	–4.870
	303			–5.690
	313			–7.331
	323			–8.972

As seen in Table 3, the positive ΔH° values indicated that the adsorption was endothermic. Moreover, these results were confirmed by the temperature effect study, where the adsorption efficiencies increased with increasing temperature. Furthermore, having positive ΔH° values indicated monolayer adsorption. The obtained values for ΔG°, as shown in Table 3, were negative. Therefore, the adsorption processes were feasible and spontaneous for all of the studied dyes.[38] The positive values for ΔS° implied an increase in randomness and the affinity of the adsorbent for the dye molecules.[38,43]

2.10. Adsorption isotherms

The adsorption isotherms were plotted to discover the correlation between the amount of adsorbed species and remaining concentration in the solution under equilibrium conditions. The Langmuir isotherm identifies monolayer adsorption assuming that the adsorption energy stays constant.[14] The Freundlich isotherm provides information on whether the adsorption is multilayer and heterogenic. The Langmuir, Freundlich, and Dubinin–Radushkevich (DR) isotherm models were applied to the equilibrium data, and the Langmuir and Freundlich isotherms were evaluated using Eqs. (8) and (9), respectively:

$$\frac{C_2}{q} = \left(\frac{1}{Q_{\max}}\right) C_2 + \frac{1}{bQ_{\max}} \tag{8}$$

$$\log q = \log K + \frac{1}{n} \log C_2 \tag{9}$$

Here, C_2 is the equilibrium concentration of the solution (mg/L), q is the amount of adsorbed dye/amount of adsorbent (mg/g), b is the Langmuir constant (L/mg), Q_{max} is the monolayer adsorption capacity (mg/g), K is the Freundlich constant (adsorption capacity (mg/g)), and 1/n is a dimensionless Freundlich constant for the intensity of the adsorbent.

The highest correlation coefficients were obtained using Langmuir isotherms. This finding indicated that all of the adsorptions were monolayer on homogeneous sites. According to Langmuir isotherms, the maximum adsorption capacities of MB, BCB, MV, PS, and BG were calculated to be 66.7, 88.5, 144.9, 56.2, and 147.1 mg/g, respectively. The DR isotherm was plotted for understanding the adsorption type using Eq. (10):

$$\ln \mathbf{Q} = \mathbf{\ln Q_{max} - k\varepsilon^2} \tag{10}$$

Here, ? (Polanyi potential) is ($RT\ln(1 + 1/C_2)$), Q is the amount of dye adsorbed per unit weight of adsorbent (mol/g), Q_{max} is the adsorption capacity (mol/g), C_2 is the equilibrium concentration of the dye in an aqueous solution (mol/L), k is a constant related to adsorption energy (mol^2/kJ^2), R is the gas constant (kJ/mol K), and T is absolute temperature (K).

The mean free energy of adsorption (E), which is defined as the free energy change when one mole of ion is transferred to the surface of a solid from infinite space in solution, can be calculated from the k value using Eq. (11):

$$\mathbf{E} = (\mathbf{2k})^{\mathbf{-0.5}} \tag{11}$$

The value of E (kJ/mol) is used for predicting the type of adsorption. When the value is below 8 kJ/mol, physical adsorption occurs. When the value is between 8 kJ/mol and 16 kJ/mol, the adsorption is actualized by chemisorption or ion exchange. As shown in Table 4, the values of E were in the range of 8 kJ/mol to 16 kJ/mol and show that the adsorption mechanism was chemical or ion exchange.

To predict the adsorption efficiency of the adsorption process, the dimensionless equilibrium parameter was determined using the following equation:

$$\mathbf{R_L} = \left(\frac{\mathbf{1}}{\mathbf{1 + bC_1}}\right) \tag{12}$$

Here, C_1 is the initial concentration and b is the Langmuir isotherm constant. R_L values of <1 indicate favorable adsorption; when the values are >1, adsorption is unfavorable. The calculated data and the relevant graphs are given in Table 4 and Figures 7a–7d. The R_L values of <1 indicated that the adsorption was favorable for all of the dyes.

2.11. Conclusions

The removal of the five cationic textile dyes from water was successfully executed using the magnetic Ni/Ni_xB-NPCR. Unlike many other adsorbents, the removal efficiencies of the five dyes were found to be advantageously independent of the initial pH. The optimum adsorbent doses were selected as 1.2 g/L for BG, 1.8 g/L for PS and MB, and 2.4 g/L for BCB and MV. The removal efficiencies reached a plateau after 60 min for PS, MB, and BG and 240 min for BCB and MV. The adsorption kinetics of MB, BG, BCB, PS, and MV showed

Table 4. The constants of Langmuir, Freundlich, and DR isotherms for MB, BG, BCB, PS, and MV adsorption using the magnetic Ni/Ni_xB-NPCR.

	MB	BCB	MV	PS	BG
Langmuir isotherm					
Q_{max} (mg/g)	66.67	88.50	144.9	56.18	147.1
b (L/mg)	6.000	0.2316	0.1239	1.728	0.3863
R^2	0.9997	0.9743	0.9899	0.9999	0.9994
Freundlich isotherm					
n	3.378	1.282	1.890	0.9966	0.9093
K (mg/g)	19.13	7.770	13.60	42.77	35.26
R^2	0.7518	0.8442	0.7841	0.9620	0.9113
DR isotherm					
E (kJ/mol)	12.50	11.62	7.217	9.806	8.704
Q_m (mol/g)	0.004433	0.003246	0.001186	0.05491	0.09945
K (mol^2/kJ^2)	0.0032	0.0037	0.0096	0.0052	0.0066
R^2	0.9238	0.9748	0.9213	0.9616	0.9091

good agreement with the pseudo second-order kinetic model. The adsorption of the dyes was well fitted to the Langmuir isotherm model and indicated monolayer adsorption on homogeneous sites. The values of E in the range of 8 kJ/mol to 16 kJ/mol showed that the adsorption mechanism was chemical or through ion exchange. Adsorption was found to be favorable for all of the dyes. The thermodynamic studies indicated that the process was endothermic, spontaneous, and feasible. A comparison of the developed adsorbent with known adsorbents from the literature can be found in Table 5. As a result, the synthesized adsorbent provided fast and effective dye removal from aqueous solutions with high adsorption capacities.

3. Experimental

3.1. Chemicals and materials

All of the chemicals used in the study were of analytical grade. Distilled water was used throughout the study. BCB (CI: 51010, MW: 317.84 g/mol, λ: 635 nm), BG (CI: 42040, MW: 482.64 g/mol, λ: 624 nm), and MB (CI: 52015, MW: 319.85 g/mol, λ: 663 nm) were obtained from Merck. MV (CI: 42535, MW: 393.95 g/mol, λ: 577 nm) and PS (CI: 50200, MW: 322.79 g/mol, λ: 520 nm) were purchased from Fluka and BDH, respectively. Acetic acid/acetate buffer (Merck), sodium hydroxide (Merck), and hydrochloric acid (Merck) were used to adjust the pH. Working dye solutions were prepared daily by diluting 1000 mg/L stock dye solutions.

Aliquots of $NiSO_4.6H_2O$ (Merck) were dissolved in 0.1 mol/L HCl to prepare 5% Ni(II) solution. Purolite C-100 cation exchange resin (0.3–1.2 mm) was used as the support material and was obtained from Purolite. A total of 4% $NaBH_4$ solution was prepared by dissolving $NaBH_4$ (Merck, 98% pure) in distilled water immediately prior to use.

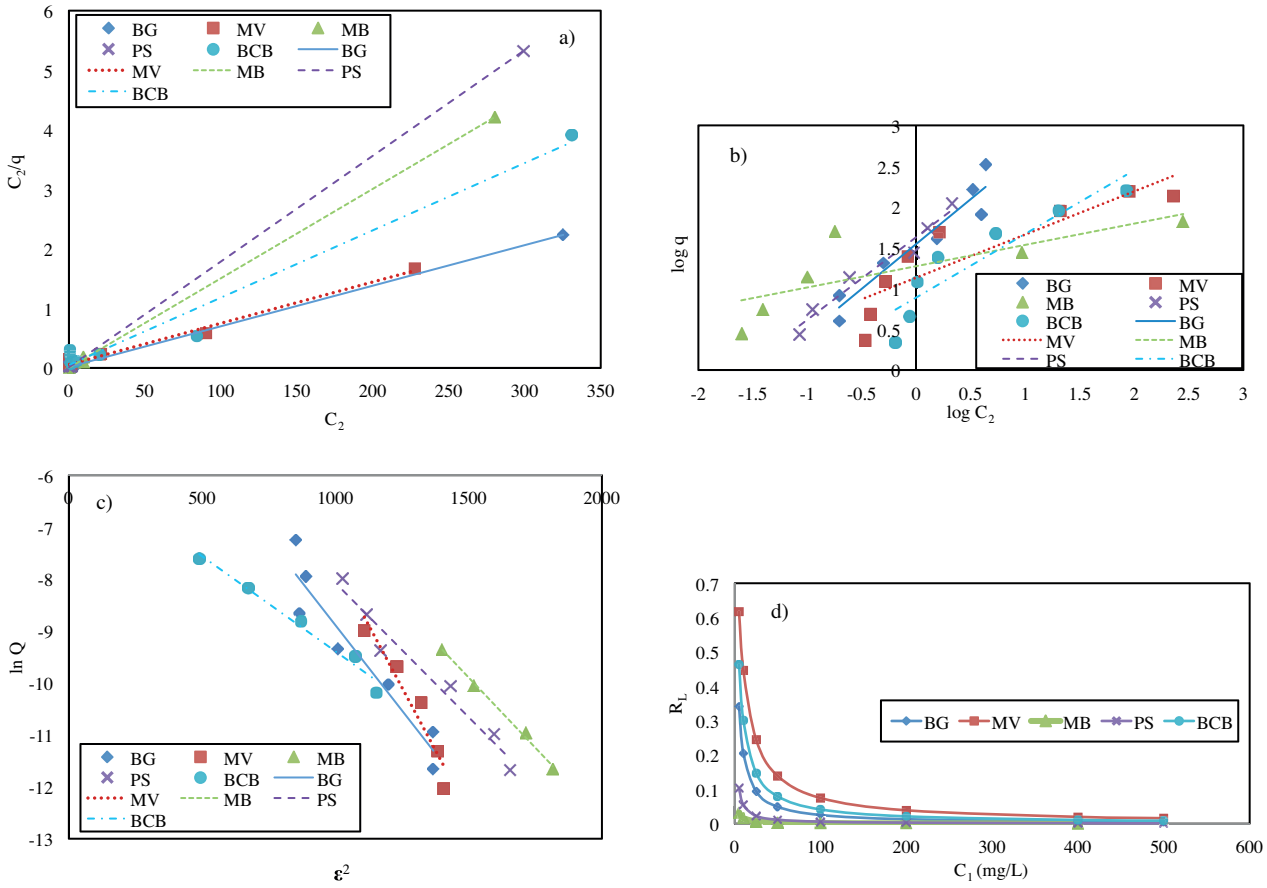

Figure 7. Langmuir isotherms (a), Freundlich isotherms (b), and DR isotherms (c) for adsorption of MB, BCB, MV, PS, and BG at equilibrium conditions, and R_L values as a function of initial dye concentrations (d) (volume: 25 mL; contact time: 60 min for PS, MB, and BG and 240 min for BCB and MV; adsorbent dose 1.2 g/L for BG, 1.8 g/L for PS and MB, 2.4 g/L for BCB and MV; temperature: 25 °C; pH: 4).

3.2. Apparatus

A Shimadzu UV-160A UV-Visible recording spectrophotometer was used for the determination of dye concentrations. pH was measured using a Mettler Toledo Five Go FG-2 pH meter. A Biosan OS-10 orbital shaker at 350 rpm and Nuve ST-402 vibration water bath were used for the adsorption studies.

3.3. Preparation of resin coated with Ni/Ni$_x$B nanoparticles

Preparation of the Ni/Ni$_x$B-NPCR was adapted from Çiftçi and Henden.[23] First, the cation exchange resin was ground and sieved. Particles in the range of 250–355 μm were then obtained. Thereafter, 2 g of resin was weighed and added to a Falcon tube. A total of 40 mL of 5% Ni(II) solution was added to the resin and shaken overnight. Excess nickel solution was decanted, and the resins were washed with distilled water several times until no reaction was observed between the remaining Ni(II) in the wash water and dimethylglyoxime. A total of 25 mL of 4% $NaBH_4$ was added to the resin drop by drop while the mixture was being stirred. After gas evolution was completed, the black Ni/Ni$_x$B-NPCR was washed with 5 mL of distilled water five times and with 5 mL of ethanol two times. The adsorbent was dried at ambient temperature.

Table 5. Comparison of the adsorbent capacity for the studied textile dyes.

Dye	Adsorbent	Q (mg/g)	Reference
Methylene blue			
	Wheat shells	16.56–21.50	[44]
	Rice husk	40.58	[13]
	Corn husk	41.55	[45]
	Graphene Nanosheet(GNS)/magnetite (Fe_3O_4) composite	43.82	[33]
	Hollow poly(cyclotriphosphazene-co-phloroglucinol) microspheres	50.7	[46]
	Ni/Ni_xB nanoparticles coated resin	66.7	This study
Methyl violet			
	Nanostructured carbon-covered sand	49.03	[29]
	Porous poly-melamine formaldehyde polymer	113.9	[47]
	Activated cotton stalks (CSAC)	135.14	[37]
	Ni/Ni_xB nanoparticles coated resin	144.9	This study
	Magnetic walnut shell	147.7	[28]
Brilliant green			
	Saklıkent mud	9.7	[38]
	Luffa cylindrical sponge	18.2	[48]
	Amine-modified tannin gel	20.41	[26]
	Peganum harmala L. seeds	35.97	[27]
	Kaolin	65.42	[2]
	Ni/Ni_xB nanoparticle-coated resin	147.1	This study
Brilliant cresyl blue			
	Natural clay	42	[49]
	Ni/Ni_xB nanoparticle-coated resin	88.5	This study
	Activated cotton stalks (CSAC)	222.22	[37]
Phenosafranine			
	Ni/Ni_xB nanoparticle-coated resin	56.2	This study
	Carboxylic-functionalized mesoporous silica	109	[50]

3.4. Dye adsorption studies

The adsorption experiments were performed in batch mode. Unless otherwise stated, 25 mL of 20 mg/L dye solutions were shaken with 30 (for BG), 45 (for PS and MB), and 60 mg (for BC and MV) adsorbents at ambient temperature for 60 (for BG, PS, and MB) and 240 min (for BCB and MV). To determine the optimum experimental conditions in the first step, 25 mL of dye solutions at different concentrations were shaken with 10 mg of sorbent for 24 h. After shaking for the optimum time, the dye-adsorbed Ni/Ni_xB nanoparticle-coated resin was separated magnetically. The remaining concentrations of dyes in the solutions were measured by a spectrophotometer at the maximum wavelength for each dye. In this case, three sets of experiments were conducted simultaneously. The pH levels of the model solutions and standards were adjusted to 5.50 with acetic acid buffer before spectrophotometric measurements.

The effect of pH on the removal efficiencies was studied in the pH range of 3 to 10 using 10 mg of sorbent for shaking for 24 h. The initial pH of the solutions was adjusted to the desired value using NaOH or HCl. The optimization studies, such as adsorbent dose (0.2, 0.4, 0.6, 1.2, 1.8, 2.4, and 4 g/L), contact time (0, 5, 10, 15, 20, 40, 60, 120, 180, 240, and 1440 min), initial dye concentrations (5, 10, 25, 50, 100, 200, and 400 mg/L), and temperature (298 K, 303 K, 313 K, and 323 K) were performed. The dye removal efficiencies (R, %) and the adsorbed dye amounts (q, mg/g) were calculated using Eqs. (13) and (14), respectively:

$$R(\%) = \frac{C_i C_e}{C_i} \times 100) \tag{13}$$

$$q = \frac{(C_i C_e) \times V}{m} \tag{14}$$

Here, C_i and C_e indicate the initial and equilibrium (remained after adsorption) dye concentrations (mg/L), respectively; m is the amount of the adsorbent (g); V is the volume of the dye solution (L). Equilibrium, thermodynamic, and kinetic studies were also conducted.

3.5. Determination of point of zero charge pH

The pH_{pzc} was determined by the immersion technique. In this technique, 25 mL of 0.1 mol/L KNO_3 solution was adjusted to different pH values using HCl or NaOH and was added to the adsorbents. Thereafter, the suspension was shaken for 24 h to obtain the equilibrium pH. The change of pH during equilibrium was calculated by subtracting the initial pH values from the final pH values. The ΔpH values were then plotted against the initial pH values. The initial pH at which the ΔpH was zero was taken to be the pH_{pzc}.

References

1. Gupta, V. K.; Suhas. *J. Environ. Manage.* **2009**, *90*, 2313-2342.
2. Nandi, B. K.; Goswami, A.; Purkait, M. K. *Appl. Clay Sci.* **2009**, *42*, 583-590.
3. Banat, I. M.; Nigam, P.; Singh, D.; Marchant, R. *Bioresour. Technol.* **1996**, *58*, 217-227.
4. Machado, F. M.; Bergmann, C. P.; Lima, E. C.; Royer, B.; de Souza, F. E.; Jauris, I. M.; Calvete, T.; Fagan, S. B. *Phys. Chem. Chem. Phys.* **2012**, *14*, 11139-11153.
5. Arami, M.; Limaee, N. Y.; Mahmoodi, N. M.; Tabrizi, N. S. *J. Colloid Interf. Sci.* **2005**, *288*, 371-376.
6. Mittal, A.; Gajbe, V.; Mittal, J. *J. Hazard. Mater.* **2008**, *150*, 364-375.
7. Yagub, M. T.; Sen, T. K.; Afroze S.; Ang, H. M. *Adv. Colloid Interfac.* **2014**, *209*, 172-184.
8. Mittal, A.; Kaur, D.; Mittal, J. *J. Colloid Interf. Sci.* **2008**, *326*, 8-17.
9. Din, M. I.; Hussain, Z.; Munir, H.; Naz, A.; Intisar, A.; Makshoof, M. N.; Mirza, M. L. *Int. J. Phytoremediat.* **2016**, *18*, 477-486.
10. Shakoor, S.; Nasar, A. *J. Taiwan Inst. Chem. E.* **2016**, *66*, 154-163.
11. Santa Cruz Biotechnology. *Material Safety Data Sheet, Phenosafranin, sc-215703*; Santa Cruz Biotechnology: Santa Cruz, CA, USA, 2009.
12. Zucca, P.; Neves, C. M. B.; Simoes, M. M. Q.; Neves, M. D. G. P. M. S.; Cocco, G.; Sanjust, E. *Molecules* **2016**, *21*, 1-40.
13. Vadivelan, V.; Vasanth Kumar, K. *J. Colloid Interf. Sci.* **2005**, *286*, 90-100.

14. Oguntimein, G. B. *J. Environ. Chem. Eng.* **2015**, *3*, 2647-2661.
15. Crini, G. *Bioresource Technol.* **2006**, *97*, 1061-1085.
16. Sanghi, R.; Bhattacharya, B. *Color. Technol.* **2002**, *118*, 256-269.
17. Madrakian, T.; Afkhami, A.; Ahmadi, M. *Spectrochim. Acta A* **2012**, *99*, 102-109.
18. Gong, J.; Wang, B.; Zeng, G. M.; Yang, C. P.; Niu, C. G.; Niu, Q.; Zhou, W. J.; Liang, Y. *J. Hazard. Mater.* **2009**, *164*, 1517-1522.
19. Rocher, V.; Siaugue, J. M.; Cabuil, V.; Bee, A. *Water Res.* **2008**, *42*, 1290-1298.
20. Hosseini, F.; Sadighian, S.; Hassan H. M.; Mahmoodi, N. M. *Desalin. Water Treat.* **2016**, *57*, 24378-24386.
21. Sahraei, R.; Hemmati, K.; Ghaemy, M. *RSC Adv.* **2016**, *6*, 72487-72499.
22. Mahmoodi, N. M.; Abdi, J.; Bastani, D. *J. Environ. Health Sci.* **2014**, *12*, 1-10.
23. Çiftçi, T. D.; Henden, E. *Powder Technol.* **2015**, *269*, 470-480.
24. Henden, E.; İşlek, Y.; Kavas, M.; Aksuner, N.; Yayayürük, O.; Çiftçi T. D.; İlktaç, R. *Spectrochim. Acta B* **2011**, *66*, 793-798.
25. Fiol, N.; Villaescusa, I. *Environ. Chem. Lett.* **2009**, *7*, 79-84.
26. Akter, N.; Hossain, A.; Hassan, M. J.; Amin, M. K.; Elias, M.; Rahman, M. M.; Asiri, A. M.; Siddiquey I. A.; Hasnat, M. A. *J. Environ. Chem. Eng.* **2016**, *4*, 1231-1241.
27. Agarwal, S.; Gupta, V. K.; Ghasemi M.; Azimi-Amin, J. *J. Mol. Liq.* **2017**, *231*, 296-305.
28. Ashrafi, M.; Arab Chamjangali, M.; Bagherian, G.; Goudarzi, N. *Spectrochim. Acta A* **2017**, *171*, 268-279.
29. Moradi, S.; Azizian, S. *J. Mol. Liq.* **2016**, *219*, 909-913.
30. Altıntıg, E.; Altundag, H.; Tuzen, M.; Sarı, A. *Chem. Eng. Res. Des.* **2017**, *122*, 151-163.
31. Afkhami, A.; Moosavi, R. *J. Hazard. Mater.* **2010**, *174*, 398-403.
32. Gemeay, A. H.; Mansour, I. A.; El-Sharkawy, R. G.; Zaki, A. B. *J. Chem. Technol. Biot.* **2004**, *79*, 85-96.
33. Ai, L.; Zhang, C.; Chen, Z., *J. Hazard. Mater.* **2011**, *192*, 1515-1524.
34. Chowdhury, S.; Chakraborty, S.; Saha, P. *Colloid. Surface. B* **2011**, *84*, 520-527.
35. Üner, O.; Geçgel, Ü.; Bayrak, Y. *Water Air Soil Poll.* **2016**, *7*, 227-247.
36. Fil, B. A.; Korkmaz, M.; Özmetin, C. *J. Disper. Sci. Technol.* **2016**, *37*, 991-1001.
37. Özdemir, M.; Durmuş, Ö.; Şahin, Ö.; Saka, C. *Desalin. Water Treat.* **2016**, *57*, 18038-18048.
38. Kismir, Y.; Aroguz, A. Z. *Chem. Eng. J.* **2011**, *172*, 199-206.
39. Mandal, B.; Ray, S. K. *J. Taiwan Inst. Chem. E.* **2016**, *60*, 313-327.
40. Luo, W. J.; Gao, Q.; Wu, X. L.; Zhou, C. G. *Sep. Sci. Technol.* **2014**, *49*, 2400-2411.
41. El Haddad, M.; Regti, A.; Slimani, R.; Lazar, S. *J. Ind. Eng. Chem.* **2014**, *20*, 717-724.
42. Ho, Y. S.; McKay, G. *Chem. Eng. J.* **1998**, *70*, 115-124.
43. Allen, S. J.; Gan, Q.; Matthews, R.; Johnson, P. A. *J. Colloid Interf. Sci.* **2005**, *286*, 101-109.
44. Bulut, Y.; Aydin, H. *Desalination* **2006**, *194*, 259-267.
45. Paska, O. M.; Acurariu, C. P.; Muntean, S. G. *RSC Adv.* **2014**, *4*, 62621-62630.
46. Fu, J.; Chen, Z.; Wu, X.; Wang, M.; Wang, X.; Zhang J.; Zhang, J. *Chem. Eng. Jpn.* **2015**, *281*, 42-52.
47. Wang, Y.; Xie, Y.; Zhang, Y.; Tang, S.; Guo, C.; Wu J.; Lau, R. *Chem. Eng. Res. Des.* **2016**, *114*, 258-267.
48. Esan, O. S.; Abiola, O. N.; Owoyomi, O.; Aboluwoye, C. O.; Osundiya, M. O. *ISRN Phys. Chem.* **2014**, *2014*, 743532.
49. İyim, T. B.; Güçlü, G. *Desalination* **2009**, *249*, 1377-1379.
50. Yan, Z.; Tao, S.; Yin, J.; Li, G. *J. Mater. Chem.* **2006**, *16*, 2347-2353.